

# Pseudotachylyte increases the post-slip strength of faults

B. Proctor and D.A. Lockner

U.S. Geological Survey, Earthquake Science Center, 345 Middlefield Road, MS977, Menlo Park, California 94025, USA

## ABSTRACT

Solidified frictional melts, or pseudotachylytes, are observed in exhumed faults from across the seismogenic zone. These unique fault rocks, and many experimental studies, suggest that frictional melting can be an important process during earthquakes. However, it remains unknown how melting affects the post-slip strength of the fault and why many exhumed faults do not contain pseudotachylyte. Analyses of triaxial stick-slip events on Westerly Granite (Rhode Island, USA) sawcuts at confining pressures from 50 to 400 MPa show evidence for frictional heating, including some events energetic enough to generate surface melt. Total and partial stress drops were observed with slip as high as 6.5 mm. We find that in dry samples following melt-producing stick slip, the shear failure strength increased as much as 50 MPa, while wet samples had <10 MPa strengthening. Microstructural analysis indicates that the strengthening is caused by welding of the slip surface during melt quenching, suggesting that natural pseudotachylytes may also strengthen faults after earthquakes. These results predict that natural pseudotachylyte will inhibit slip reactivation and possibly generate stress heterogeneities along faults. Wet samples do not exhibit melt welding, possibly because of thermal pressurization of water reducing frictional heating during slip.

## INTRODUCTION

Abundant field, laboratory, and theoretical evidence supports the occurrence of frictional melting during earthquake slip, suggesting that solidified melt or pseudotachylyte is periodically generated within some fault zones (e.g., Sibson, 1975; Rice, 2006; Kirkpatrick et al., 2009; Spray, 2010; Niemeijer et al., 2011). Subsequent earthquakes will occur when the stress due to tectonic loading reaches the fault strength, which is presumed to increase more rapidly than post-seismic loading. To date it remains unknown how the presence of pseudotachylyte affects the post-seismic strength of fault rocks, and how it may contribute to the temporal distribution and magnitude of subsequent earthquakes. Furthermore, it remains unclear why many fault zones apparently do not contain pseudotachylyte (e.g., Sibson and Toy, 2006; Kirkpatrick et al., 2009).

Stick slip is a dynamic frictional sliding phenomenon that underlies prominent models of natural earthquakes (e.g., Brace and Byerlee, 1966; Scholz, 2002). Under appropriate laboratory conditions using a triaxial press, melting can be achieved during slip events with displacements on the order of a few millimeters (Lockner et al., 2017; Brantut et al., 2016). These events provide an advantageous laboratory method for studying strengthening effects associated with frictional melting compared with conventional rotary machines (e.g., Niemeijer et al., 2011) because orders of magnitude less displacement (and time) are required to both generate melt and arrest slip. This approach provides a quasi-closed system for fluids trapped within the fault

and limits gouge production and microstructural overprinting that can occur during longer slip events (e.g., Proctor et al., 2014).

In this study, we report results from stick-slip experiments on Westerly Granite (Rhode Island, USA) under dry and wet conditions. Using a novel experimental procedure and microstructural observations we explore how and why fault strength evolves following stick-slip events energetic enough to generate surface melt. These tests allow us to interpret field observations from pseudotachylyte-bearing faults and

further constrain how water affects frictional melting in natural faults.

## METHODS

Room-temperature experiments were performed on Westerly Granite in a conventional triaxial apparatus (see the GSA Data Repository<sup>1</sup>). Cylindrical cores, 2.54 cm in diameter by ~6.4 cm long, were first sawcut at 30° ( $\theta$ ) to the axial loading direction. The sawcut surfaces were leveled with a surface grinder and hand-lapped with 600 grit alumina abrasive. An ~3.8-mm-thick polyurethane jacket was used to isolate the sample from the kerosene confining fluid (Fig. 1A). All mechanical data were recorded at 1 Hz.

To induce stick-slip frictional sliding, 36 samples were loaded under computer control at a constant effective confining pressure ( $\bar{\sigma}_3 = \sigma_3 - P_f$ , where  $P_f$  is pore fluid pressure) of 50–400 MPa and a constant axial shortening rate ( $\dot{v}$ ) of 5  $\mu\text{m/s}$ . The inclined fault remained locked until

<sup>1</sup>GSA Data Repository item 2016337, description of deformation apparatus, methods and data reduction, summary of experimental conditions, description of starting material, mechanical data, and additional observations of experimental microstructures, is available online at [www.geosociety.org/pubs/ft2016.htm](http://www.geosociety.org/pubs/ft2016.htm), or on request from [editing@geosociety.org](mailto:editing@geosociety.org).

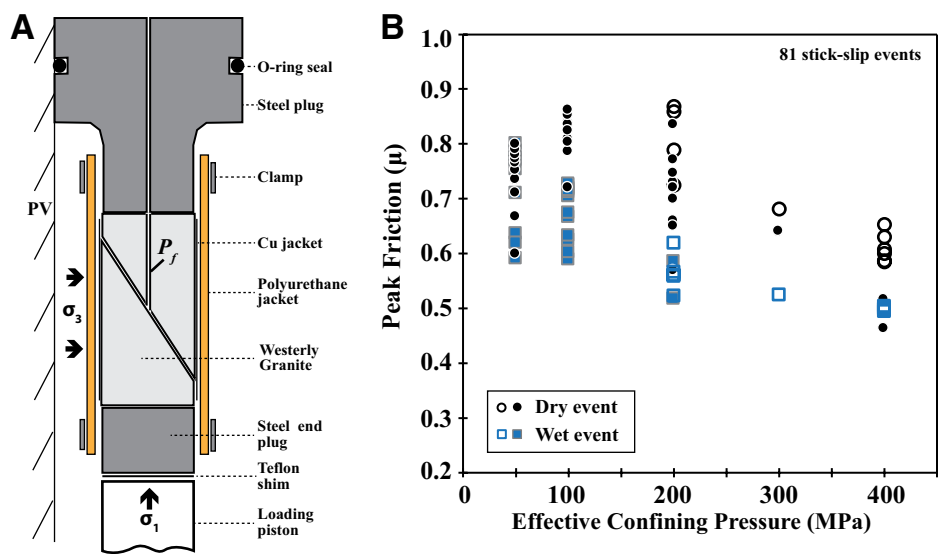


Figure 1. A: Schematic diagram of the sample assembly within a triaxial press pressure vessel (PV).  $P_f$  notes the pore fluid pressure port. B: Plot of peak friction values measured at the onset of stick-slip events. Solid symbols indicate a partial stress drop and open symbols indicate a total stress drop during stick-slip events.

slip initiated spontaneously. During the stick-slip events the slip velocities were not measured, but likely surpassed 1 m/s with event durations of 0.1–0.3 ms (Lockner et al., 2017). Dry runs were performed at room-dry conditions. In wet runs, faults were pressurized with deionized water via a 2.4 mm port cored through the top granite piece (e.g., Fig. 1A). In most runs, the pore fluid pressure was set to 5% of  $\bar{\sigma}_3$ . To investigate how the fault strength evolved following a slip-slip event, we reloaded 18 samples at a lower confining pressure and imposed a constant effective normal stress ( $\bar{\sigma}_n = \sigma_n - P_f$ ) of 60 MPa, which is the lowest value that could be maintained. For these strength recovery tests, the samples were first brought to hydrostatic conditions by reducing the axial stress and manually lowering  $\bar{\sigma}_3$  to 60 MPa over 5–10 min. Then, under computer control,  $\bar{\sigma}_n$  was maintained at 60 MPa and a constant axial shortening rate of 1  $\mu\text{m/s}$  was imposed. The total time between stick-slip events and reloading ranged from 17 to 41 min. For comparison, we also performed 4 strength recovery tests with  $\bar{\sigma}_3 = 50$  MPa and  $v = 5 \mu\text{m/s}$  and 2 control tests on samples that did not undergo stick-slip events (see the Data Repository).

Microimaging of the slip surface was conducted on selected samples with a Tescan VEGA 3 scanning electron microscope using secondary electrons. The imaged samples were separated along the sawcut and loose gouge was removed with either compressed air for dry runs or distilled water for wet runs.

## RESULTS

The peak coefficient of friction values ( $\mu = \tau / \bar{\sigma}_n$ , where  $\tau$  and  $\bar{\sigma}_n$  are shear and effective normal stress on the fault) from 81 stick-slip events are shown in Figure 1B. At  $\bar{\sigma}_3 = 50$  MPa, both wet and dry samples had similar friction values that ranged from ~0.6 to 0.8. At higher confining pressures, the dry samples had friction values that, on average, were ~20% larger than wet samples. The slip events were accompanied by both partial (solid symbols in Fig. 1B) and total (open symbols) stress drops. For samples that underwent multiple stick-slip events, wet runs almost always underwent a total stress drop during the first slip event at  $\bar{\sigma}_3 \geq 200$  MPa, whereas dry runs typically underwent one or more partial events prior to achieving a total stress drop event (see the Data Repository).

Five representative stick-slip events and one control run are shown in Figure 2A for samples deformed at  $\bar{\sigma}_3 = 400$  MPa. Of the 5 samples, 4 underwent total stress drop events with fault slip values ( $\delta$ ) as high as 6.5 mm. Total stress drop occurs when slip exceeds the elastic elongation of the piston and a gap appears between the piston and the bottom end plug (e.g., Lockner et al., 2017). One dry sample (run 45) exhibited a partial stress drop (orange trace) with  $\delta \approx 1.2$  mm. The linear unloading profiles shown

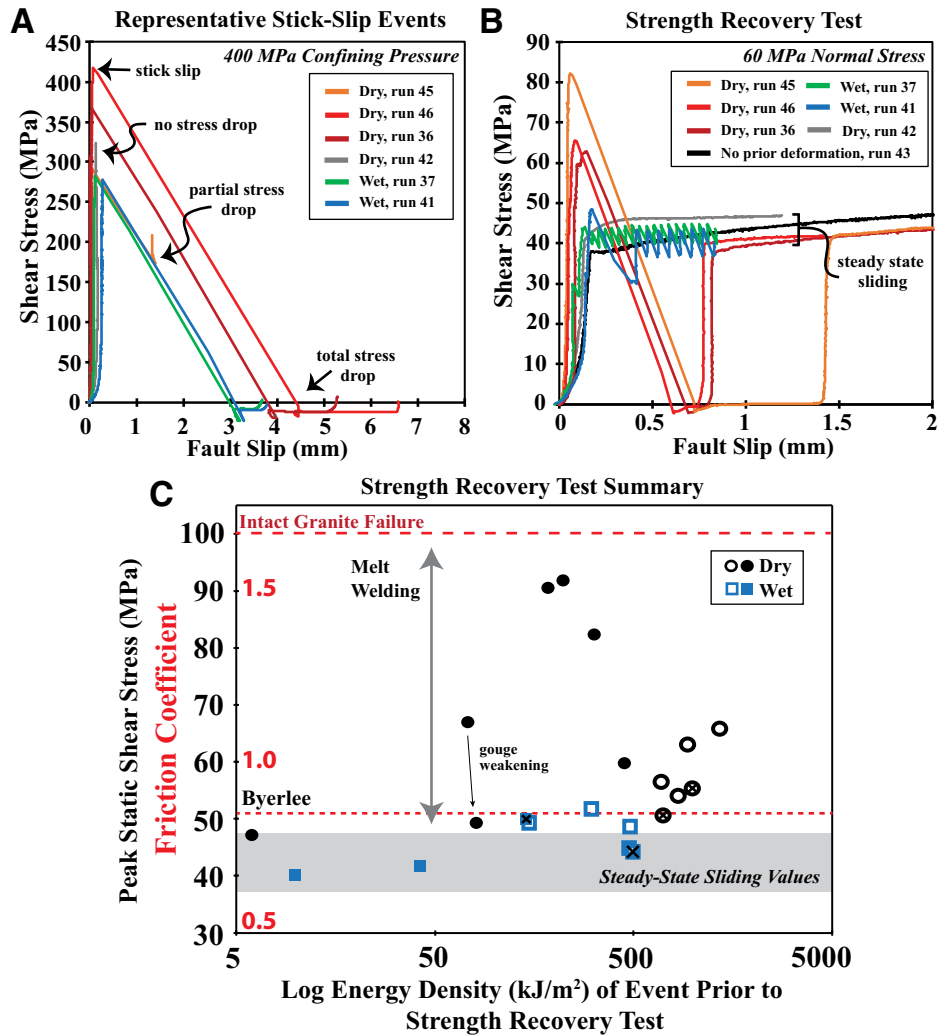


**Figure 2. A:** Graph showing results of representative experiments conducted at 400 MPa confining pressure. **B:** Graph showing results of strength recovery tests following events shown in A. Fault displacement at the onset of loading was set to zero. **C:** Plot of peak shear stress values obtained during strength recovery tests as a function of the energy density released during the preceding stick-slip events (see text). Open (total) and solid (partial) symbols note the magnitude of the prior stress drops. Symbols denoted with x indicate stress values normalized from strength recovery tests performed with a constant confining pressure (see the Methods discussion in text). Byerlee friction is 0.85 and the granite failure strength is ~100 MPa at these conditions (Lockner and Beeler, 2002).

in Figure 2A are artifacts of the 1 Hz recording rate. Previous work has shown that stick-slip events exhibit highly nonlinear unloading with durations of 0.1–0.3 ms (Lockner et al., 2017).

Following each slip event, we conducted strength recovery tests (see the Methods discussion). Strength recovery tests (SR tests), shown in Figure 2B, allowed us to directly compare restrengthening for slip events conducted at different confining pressures. During these SR tests, both wet and dry samples exhibited elastic strengthening to a peak shear stress value, which was followed by a dynamic stress drop and then quasi-steady-state sliding (Fig. 2B). The peak stress values and static stress drop magnitudes were consistently larger for dry samples than for wet samples. The dry samples were as much as 50 MPa stronger than the steady-state sliding

values (38–45 MPa) and underwent total stress drops during reloading (Fig. 2B), in stark contrast to the stable sliding exhibited by a dry sample that had no prior deformation (run 43 black trace, Fig. 2B). Likewise, a dry sample that underwent axial loading at  $\bar{\sigma}_3 = 400$  MPa, but was unloaded without a stick-slip event (run 42 gray trace, Fig. 2B), did not exhibit a stress drop during the subsequent SR test. Log-time strength recovery in slide-hold-slide tests would be <1 MPa for these conditions.

In Figure 2C the peak stress (and friction) values measured during all SR tests are plotted against the normalized energy released ( $E_r$ ) during the prior slip event;  $E_r$  was calculated as

$$E_r = \frac{F_{av} \delta \cos \theta}{A}, \quad (1)$$

where  $F_{av}$  is the average axial force during the slip event with displacement  $\delta$  and  $A$  is the slip surface area. Work expended compressing the confining fluid ( $\int \sigma_3 dV$ ) has been removed (e.g., Lockner et al., 2017). The  $E_f$  values are reported as energy densities and correlate with an average temperature increase on the fault during stick-slip sliding (Lockner et al., 2017). Figure 2C shows that dry samples that experienced energy densities  $> \sim 50$  kJ/m<sup>2</sup> have enhanced peak stress values relative to their steady-state sliding values. Samples that underwent partial stress drops (solid symbols in Fig. 2C) had the highest peak stress values, which approach the strength of intact Westerly Granite ( $\sim 100$  MPa; e.g., Lockner and Beeler, 2002). The highest peak stress (92 MPa;  $\mu \approx 1.5$ ) was attained in a dry sample (at  $\bar{\sigma}_3 = 200$  MPa) that underwent a partial stress drop. Conversely, wet samples had little to no post-slip strengthening over the range of energy densities tested.

Microstructural investigation of the slip surface revealed evidence for melting in both wet and dry experiments slipped at  $\bar{\sigma}_3 \geq 100$  MPa (see the Data Repository). The apparently once molten material occurred in an  $\sim 1$ - $\mu$ m-thick layer on the slip surface and contained vesicles, entrained clasts, and finger-like flow structures (Fig. 3A), consistent with previously reported melt textures (e.g., Moore et al., 2016; Proctor et al., 2014) and with thermal modeling results from experiments under similar conditions (Lockner et al., 2017). At  $\bar{\sigma}_3 = 100$  MPa, the melt material occurred in patches (see the Data Repository), while at higher confining pressures the entire slip surface was covered with melt material (as best inferred from microstructures).

In general, the apparent volume of melt material on wet samples was notably less than on dry samples slipped at the same confining pressures. Furthermore, on dry samples we observed remnant sections of the facing shear block (now removed) that were melt welded to the slip surface (Fig. 3B). We also noted missing sections of the slip surface that were presumably welded to the opposing shear block (Fig. 3B). These welded structures added topographic relief to the slip surfaces and were more abundant in samples deformed at higher confining pressures, such that at  $\bar{\sigma}_3 = 400$  MPa the melt-covered (syn-slip) surfaces were only observed in isolated windows (see the Data Repository). Conversely, the wet samples did not exhibit welded structures, even at the highest confining pressures tested (see the Data Repository); those post-slip slip surfaces remained remarkably flat.

## DISCUSSION

We propose that frictional melting and subsequent welding (melt welding) along the slip surface in dry samples provide added cohesion that increases the post-slip failure strength. This is supported by the observations of melt textures

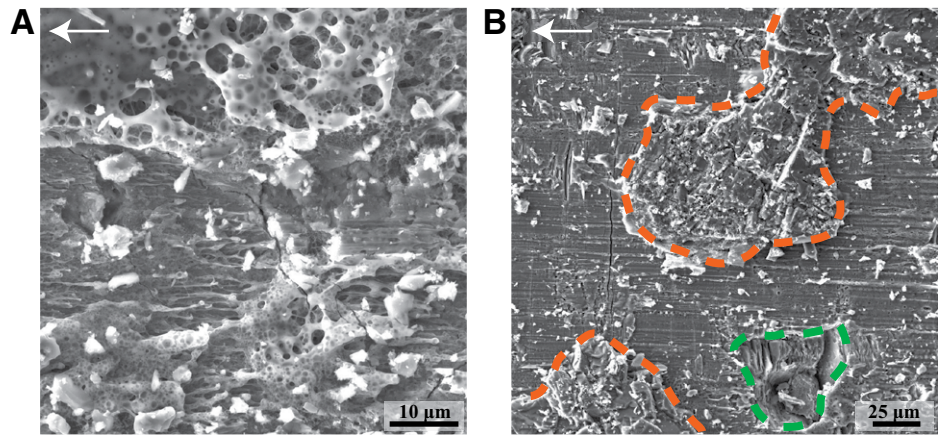


**Figure 3. Secondary electron images of the slip surface from run 14 ( $\sigma_3 = 200$  MPa). White arrows indicate the approximate slip direction of the imaged surface. A: Image of vesicle-rich patches of melt rising above a melt-covered surface with striations. The striations are defined by finger-like melt stringers that appear to be attenuated during shearing of the surface. Bright regions of the image are an artifact of surface charging during viewing. B: Image showing a melt-covered surface with striations. Dashed orange lines highlight topographically higher regions that are interpreted to be welded remnants of the facing slip surface (now detached). Conversely, the green dashed line encircles a topographically lower region (plucked out grains) that exposes fractured granite below the slip surface.**

and welding at conditions where large peak stresses during the SR tests were observed. Once the welded zones are fractured during the SR tests, all samples exhibit a similar restrengthening path and steady-state sliding strength. Melt welding also explains the progressively increasing peak stresses observed in many dry samples that underwent multiple stick-slip events at  $\bar{\sigma}_3 \geq 100$  MPa (see the Data Repository). For dry samples, the melt production rate is likely the primary factor controlling stress drop magnitude during stick-slip events (Lockner et al., 2017).

The production of gouge, in addition to melt, during slip may partially explain the lack of a positive dependence of peak strength with energy density during SR tests (Fig. 2C; i.e., bigger energy events should produce stronger samples). To explore how gouge affects melt welding, we compared a dry sample that underwent two stick-slip events at  $\bar{\sigma}_3 = 100$  MPa (run 50) to another sample that underwent six stick-slip events at otherwise identical conditions (run 51; see the Data Repository). The six-event sample had an  $\sim 38\%$  lower peak stress despite undergoing a larger energy event (Fig. 2C). Visual inspection after these SR tests revealed more gouge on the sample that underwent more slip events (see the Data Repository), suggesting that extra gouge on the surface was inhibiting melting and/or melt welding. This is further supported by a strong negative dependence of measured peak strengths during SR tests with slip prior to the tests (see the Data Repository). It remains unclear how gouge limits post-slip strengthening. It could inhibit or delay melting by lowering the slip zone strain rate (e.g., Cardwell et al., 1978) or possibly render the welding process less efficient by acting as a weak barrier between the melt

and the solid shear blocks. Off-fault damage and silica gel (Goldsby and Tullis, 2002) are additional factors that might affect the post-slip strength of our samples. Off-fault damage was not explored in this study, and Goldsby and Tullis (2002) reported no post-slip effects due to gel, so we think it is unlikely that gel significantly affected our results.

The lack of post-slip strengthening observed in wet samples is primarily caused by a lack of melting and melt welding on the slip surface (as observed in our microstructures). This result is surprising given that the melting temperature for wet granite is lower than that for dry granite (e.g., Philpotts and Ague, 2009) and suggests that additional weakening mechanisms might be active in these samples. However, it remains unclear what mechanisms are inhibiting melting and/or welding. The relatively small volume of water on the fault can absorb at most a few joules of energy ( $\ll 1\%$  of  $E_f$  in most runs), making it unlikely that water is simply absorbing enough heat to inhibit melting. Another possibility is that pore water became overpressurized during the stick-slip events via thermal pressurization (e.g., Rice, 2006; Noda et al., 2009), which would promote dilation of the slip surface and inhibit frictional heating and melt welding. An added component of thermal pressurization may explain how wet samples can undergo total stress drop events at the same (or smaller) stress values where dry samples only undergo partial stress drops (see the Data Repository). Likewise, a transient increase in water pressure might explain why stick-slip events in wet samples tend to initiate at lower shear stress values compared with dry samples (see the Data Repository). Here we propose that loss of pore

volume occurs at the onset of frictional yielding due to the collapse and comminution of surface asperities. This is supported by the observation that wet samples almost always undergo relatively little fault creep compared to dry samples prior to the nucleation of slip events (see the Data Repository).

Pseudotachylytes are commonly observed in faults crosscutting exhumed intrusive igneous and metamorphic rocks (e.g., Sibson, 1975; Swanson, 1988; Sibson and Toy, 2006). In some fault zones, pseudotachylytes occur in complex fracture networks (e.g., Swanson, 1988) or along parallel fractures, each representing a single event (e.g., Alder et al., 2015). The apparent tendency for slip to migrate along new fractures in pseudotachylyte-bearing faults is notably different from sections of faults without pseudotachylyte, such as within the Punchbowl fault and Alpine fault, in which slip was reactivated over many events within a narrow zone (e.g., Chester and Chester, 1998; Sutherland et al., 2012). These outcrop-scale differences may be explained by strengthening associated with pseudotachylyte formation, consistent with experiments conducted on natural pseudotachylyte samples (T.M. Mitchell, 2016, personal commun.). We propose that slip reactivation is inhibited by melt welding along the fault, such that subsequent slip is forced to nucleate along new fractures in the wall rock, similar to those observed in the Fort Foster brittle zone in south-east Maine (Swanson, 1988).

More broadly, melt welding might be an important process for generating stress heterogeneity along a fault zone, a fundamental characteristic of most faults (e.g., Rice, 1993). If, during an earthquake, melting occurs within isolated patches of the fault, the post-slip pseudotachylytes will potentially form stronger zones or asperities. The long-term mechanical impact of these zones will depend on their local susceptibility to metasomatism and plastic deformation, which is observed in exhumed lower crustal rocks (e.g., Price et al., 2012).

Many studies have proposed that frictional melting is inhibited by thermal pressurization of water within the fault during earthquake slip (e.g., Sibson, 1973; Rice, 2006; Viesca and Garagash, 2015). Our wet stick-slip experiments generally support these hypotheses and further show that there may be important post-slip strengthening effects (or a lack thereof) that should be considered when modeling the strength of faults.

## ACKNOWLEDGMENTS

We thank Nick Beeler, Brian Kilgore, Ben Melosh, Diane Moore, André Niemeijer, John Spray, Greg Walsh, and an anonymous reviewer for helpful discussions and comments, and Leslie Hayden for help running the scanning electron microscope. Any use of product names is for descriptive purposes only and does not imply endorsement by the U.S. Government.

## REFERENCES CITED

- Alder, S., Smith, S., Tesei, T., and Collettini, C., 2015, Frictional controls on high-angle reverse faulting during compressional basin inversion: Abstract MR33C-2679 presented at the 2015 Fall Meeting, American Geophysical Union, San Francisco, California.
- Brace, W.F., and Byerlee, J.D., 1966, Stick-slip as a mechanism for earthquakes: *Science*, v. 153, p. 990–992, doi:10.1126/science.153.3739.990.
- Brantut, N., Passelègue, F.X., Deldicque, D., Rouzaud, J.-N., and Schubnel, A., 2016, Dynamic weakening and amorphization in serpentinite during laboratory earthquakes: *Geology*, v. 44, p. 607–610, doi:10.1130/G37932.1.
- Cardwell, R.K., Chinn, D.S., Moore, G.F., and Turcotte, D.L., 1978, Frictional heating on a fault zone with finite thickness: *Geophysical Journal International*, v. 52, p. 525–530, doi:10.1111/j.1365-246X.1978.tb04247.x.
- Chester, F.M., and Chester, J.S., 1998, Ultracataclastic structure and friction processes of the Punchbowl fault, San Andreas system, California: *Tectonophysics*, v. 295, p. 199–221, doi:10.1016/S0040-1951(98)00121-8.
- Goldsby, D.L., and Tullis, T.E., 2002, Low frictional strength of quartz rocks at subseismic slip rates: *Geophysical Research Letters*, v. 29, 1844, doi:10.1029/2002GL015240.
- Kirkpatrick, J.D., Shipton, Z.K., and Persano, C., 2009, Pseudotachylytes: Rarely generated, rarely preserved, or rarely reported?: *Seismological Society of America Bulletin*, v. 99, p. 382–388, doi:10.1785/0120080114.
- Lockner, D.A., and Beeler, N.M., 2002, Rock failure and earthquakes, in Lee, W.H.K., et al., eds., *International handbook of earthquake and engineering seismology*: Amsterdam, Academic Press, p. 505–537, doi:10.1016/S0074-6142(02)80235-2.
- Lockner, D.A., Kilgore, B.D., Beeler, N.M., and Moore, D.E., 2017, The transition from frictional sliding to shear melting in laboratory stick-slip experiments: *American Geophysical Union Geophysical Monograph*, v. 222 (in press).
- Moore, D.E., Lockner, D.A., Kilgore, B.D., and Beeler, N.M., 2016, Gallery of melt textures developed in Westerly Granite during high-pressure triaxial friction experiments: *U.S. Geological Survey Open-File Report 2016-1059*, 75 p.
- Niemeijer, A., Di Toro, G., Nielsen, S., and Di Felice, F., 2011, Frictional melting of gabbro under extreme experimental conditions of normal stress, acceleration, and sliding velocity: *Journal of Geophysical Research*, v. 116, B07404, doi:10.1029/2010JB008181.
- Noda, H., Dunham, E.M., and Rice, J.R., 2009, Earthquake ruptures with thermal weakening and the operation of major faults at low overall stress levels: *Journal of Geophysical Research*, v. 114, B07302, doi:10.1029/2008JB006143.
- Philpotts, A., and Ague, J., 2009, *Principles of igneous and metamorphic petrology* (second edition): Cambridge, UK, Cambridge University Press, 684 p., doi:10.1017/CBO9780511813429.
- Proctor, B.P., Mitchell, T.M., Hirth, G., Goldsby, D., Zorzi, F., Platt, J.D., and Di Toro, G., 2014, Dynamic weakening of serpentinite gouges and bare surfaces at seismic slip rates: *Journal of Geophysical Research*, v. 119, doi:10.1002/2014JB011057.
- Price, N.A., Johnson, S.E., Gerbi, C.C., and West, D.P., Jr., 2012, Identifying deformed pseudotachylyte and its influence on the strength and evolution of a crustal shear zone at the base of the seismogenic zone: *Tectonophysics*, v. 518, p. 63–83, doi:10.1016/j.tecto.2011.11.011.
- Rice, J.R., 1993, Spatio-temporal complexity of slip on a fault: *Journal of Geophysical Research*, v. 98, doi:10.1029/93JB00191.
- Rice, J.R., 2006, Heating and weakening of faults during earthquake slip: *Journal of Geophysical Research*, v. 111, B05311, doi:10.1029/2005JB004006.
- Scholz, C.H., 2002, *The mechanics of earthquakes and faulting* (second edition): Cambridge, UK, Cambridge University Press, 504 p., doi:10.1017/CBO9780511818516.
- Sibson, R.H., 1973, Interactions between temperature and pore fluid pressure during earthquake faulting—a mechanism for partial or total stress relief: *Nature Physical Science*, v. 243, p. 66–68, doi:10.1038/physci243066a0.
- Sibson, R.H., 1975, Generation of pseudotachylyte by ancient seismic faulting: *Geophysical Journal International*, v. 43, p. 775–794, doi:10.1111/j.1365-246X.1975.tb06195.x.
- Sibson, R.H., and Toy, V.G., 2006, The habitat of fault-generated pseudotachylyte: Presence vs. absence of friction-melt, in Abercrombie, R., et al., eds., *Earthquakes: Radiated energy and the physics of faulting*: American Geophysical Union Geophysical Monograph 170, p. 153–166, doi:10.1029/170GM16.
- Spray, J.G., 2010, Frictional melting processes in planetary materials: From hypervelocity impact to earthquakes: *Annual Review of Earth and Planetary Sciences*, v. 38, p. 221–254, doi:10.1146/annurev.earth.031208.100045.
- Sutherland, R., et al., 2012, Drilling reveals fluid control on architecture and rupture of the Alpine fault, New Zealand: *Geology*, v. 40, p. 1143–1146, doi:10.1130/G33614.1.
- Swanson, M.T., 1988, Pseudotachylyte-bearing strike-slip duplex structures in the Fort Foster brittle zone, S. Maine: *Journal of Structural Geology*, v. 10, p. 813–828, doi:10.1016/0191-8141(88)90097-1.
- Viesca, R.C., and Garagash, D.I., 2015, Ubiquitous weakening of faults due to thermal pressurization: *Nature Geoscience*, v. 8, p. 875–879, doi:10.1038/ngeo2554.

Manuscript received 11 July 2016

Revised manuscript received 19 September 2016

Manuscript accepted 21 September 2016

Printed in USA